Available online at www.sciencedirect.com
ScienceDirect
Journal of Power Sources 174 (2007) 761–765
JOURNAL OF POWER SOURCES
www.elsevier.com/locate/jpowsour

Short communication

# *In-situ* XRD investigations on structure changes of $ZrO_2$-coated $LiMn_{0.5}Ni_{0.5}O_2$ cathode materials during charge

Bing-Joe Hwang [a,b,*], Shao-Kang Hu [a], Ching-Hsiang Chen [a], Chun-Yu Chen [a], Hwo-Shuenn Sheu [b]

[a] *Department of Chemical Engineering, National Taiwan University of Science and Technology, Taipei 10672, Taiwan*
[b] *National Synchrotron Research Center, Hsinchu 30076, Taiwan*

Available online 28 June 2007

**Abstract**

The structural changes of pristine and $ZrO_2$-coated $LiMn_{0.5}Ni_{0.5}O_2$ cathode materials were investigated by using *in situ* X-ray diffraction (XRD) during charging process. An obviously solid solution phase transition from a hexagonal structure (H1) to another hexagonal structure (H2) was observed during the charging process at a constant current of 0.3 mA in the potential range of 2.5–5.7 V. The second hexagonal structure has a shorter *a*-axis and a longer *c*-axis before the crystal collapse. Before the structure collapses the *c*-axis length increases to maximum and then significantly decreases to 14.1 Å. The *c*-axis length of the pristine and $ZrO_2$-coated $LiMn_{0.5}Ni_{0.5}O_2$ increases to the maximum at the charge capacity of 119.2 and 180.9 mAh $g^{-1}$, respectively. It can be concluded that the $ZrO_2$ coating can strongly stabilize the crystal structure of the $LiMn_{0.5}Ni_{0.5}O_2$ compound from the comparison of the lattice parameter variations between the pristine and the $ZrO_2$-coated $LiMn_{0.5}Ni_{0.5}O_2$ compounds upon charge. The potential fluctuation resulting from the decomposition of electrolytes starts at the charge capacity of around 200 and 260 mAh $g^{-1}$ for the pristine and $ZrO_2$-coated $LiMn_{0.5}Ni_{0.5}O_2$, respectively. It suggests that the $ZrO_2$ coating layer can impede the reaction between the cathode material and electrolyte.
© 2007 Elsevier B.V. All rights reserved.

*Keywords:* Structure; $LiMn_{0.5}Ni_{0.5}O_2$; Cathode; *In-situ* XRD; Charge; $ZrO_2$-coated

## 1. Introduction

Research for new cathode materials have been strongly stimulated by recent development of lithium ion batteries. Such materials are expected to deliver larger reversible capacity, with a weak capacity loss upon recharge, high structural stability and good cycleability over several hundreds of cycles. Layered lithium manganese nickel oxides have recently been shown to be promising cathode materials for use in lithium ion rechargeable batteries [1–3]. Ohzuku and Makimura showed that lithium manganese nickel oxide represents a possible alternative to $LiCoO_2$ for advanced lithium ion batteries, in terms of its operating voltage, capacity, cycleability, thermal safety, and material economy [4]. Recently lots of efforts have been reported to improve the electrochemical properties of $LiMn_{0.5}Ni_{0.5}O_2$ materials such as carbon coating [5] and doping with $Li_2TiO_3$ [6]. Surface coating has been applied to various cathode materials. Although surface coating applied in a cathode material always improves its electrochemical properties in the most of cases, the mechanism responsible for the enhancement is still unclear and on debate Chen and Dahn have indeed shown that a simple heat treatment of $LiCoO_2$ leads to similar results to those obtained for metal oxide coated sample [7]. Yang et al. [8] have reported the *in situ* XRD investigation on the layered $LiMn_{0.5}Ni_{0.5}O_2$ compounds prepared by a co-precipitated process during charging and discharging in the potential range of 3.6–4.7 V. A phase transition from a hexagonal structure (H1) to another hexagonal structure (H2) was observed during a C/17 charge to 4.7 V.

In this work, the layered $LiMn_{0.5}Ni_{0.5}O_2$ cathode materials were prepared by a sol–gel method and $ZrO_2$ layer were coated on its surface by a developed process. The *in situ* XRD was applied to investigate the crystal structural change of the pristine and the $ZrO_2$-coated $LiMn_{0.5}Ni_{0.5}O_2$ compounds upon charge in a potential range of 2.5–5.7 V. The possible mechanisms responsible for the improvement of its electrochemical properties via surface coating will be discussed.

* Corresponding author at: #43, Keelung Road, National Taiwan University of Science and Technology, Taipei 10672, Taiwan.
*E-mail address:* bjh@mail.ntust.edu.tw (B.-J. Hwang).

0378-7753/$ – see front matter © 2007 Elsevier B.V. All rights reserved.
doi:10.1016/j.jpowsour.2007.06.151

## 2. Experimental

$LiMn_{0.5}Ni_{0.5}O_2$ powders were synthesized by the sol–gel process using citric acid as a chelating agent [9–10]. A stoichiometric amount of lithium acetate ($Li(CH_3COO)\cdot 2H_2O$), nickel acetate ($Ni(CH_3COO)_2\cdot 4H_2O$), and manganese acetate ($Mn(CH_3COO)_2\cdot 4H_2O$) was dissolved in distilled water and mixed with an aqueous solution of citric acid. The resulting solution was mixed with a magnetic stirrer at 80 °C for 5–6 h to obtain a clear viscous gel. The gel was dried in a vacuum oven at 140 °C for 24 h. The $LiMn_{0.5}Ni_{0.5}O_2$ precursor was ground and calcined at 900 °C at an oxygen atmosphere. During heating and cooling, the variation of temperature was fixed at 5 °C $min^{-1}$. The $ZrO_2$-coated $LiMn_{0.5}Ni_{0.5}O_2$ was prepared by mixing the prepared $LiMn_{0.5}Ni_{0.5}O_2$ powders and $Zr(OC_3H_7)_4$ in 1-propanol solution. The entire process was carried out with stirring continuously at room temperature. The prepared solution was heated in a beaker in a temperature range of 80–90 °C until a transparent sol was obtained. The resulting precursor was sintered at 450 °C for 5 h to obtain the $ZrO_2$-coated $LiMn_{0.5}Ni_{0.5}O_2$ powders.

The Li, Ni and Mn contents in the resulting materials were analyzed using an inductively coupled plasma/atomic emission spectrometer (ICP/AES, Kontron S-35). The phase purity was verified from powder X-ray diffraction measurements (XRD, Rigaku D/max-b) using Cu $K_\alpha$ radiation. The particle morphology of the powders after calcination was obtained using a scanning electron microscopy (SEM, Hitachi S-4100). Electrochemical characterization was carried out with a coin-type cell. The synthesized pristine and the $ZrO_2$-coated $LiMn_{0.5}Ni_{0.5}O_2$ cathode film were prepared by mixing an 85:3.5:1.5:10 (w/w) ratio of active materials, carbon black, KS6 graphite and polyvinylidene fluoride binder, respectively, in *N*-methyl pyrrolidinone. The resulting paste was cast on an aluminum current collector. The entire assembly was dried under vacuum overnight and then heated in an oven at 120 °C for 2 h. Lithium metal (FMC) was used as an anode and a polypropylene separator was used to separate the anode and the cathode. 1.0 M $LiPF_6$ dissolved in a 1:1 mixture of ethylene carbonate (EC)/diethyl carbonate (DEC) was used as an electrolyte. The cells were assembled in an argon-filled dry box where both the moisture and oxygen contents were less than 1 ppm. The electrochemical measurements have been performed in the potential range of 2.5–5.7 V using programmable battery cycle tester (Maccor model 2300) at room temperature.

*In situ* X-ray diffraction (XRD) measurements were carried out at the high energy beam line 01C2 at the National Synchrotron Radiation Research Center (NSRRC), Hisnchu. The beam line was operated at energy of 25 keV. The XRD pattern was recorded using the wavelength ($\lambda$) = 0.5166 Å for limited angular regions at room temperature. The optical design for the monochromatic beam is as follows: the first mirror focusing at the beam vertically and asymmetrically cut and horizontally bendable a perfect single crystal as the diffraction object monochromatically focused the beam. A single crystal of Si(1 1 1) with about 10% asymmetric cutting was used to deliver a monochromatic beam size 1 mm in diameter with a single spot at the sample, which is about 24 and 6 m away from the source and monochromatic, respectively, flat imaging plane was used as a 2D area detector, which can collect diffraction pattern of the 2$\theta$ scale up to 40°. The XRD pattern was read out by a MAC IPR420 off line imaging plate scanner.

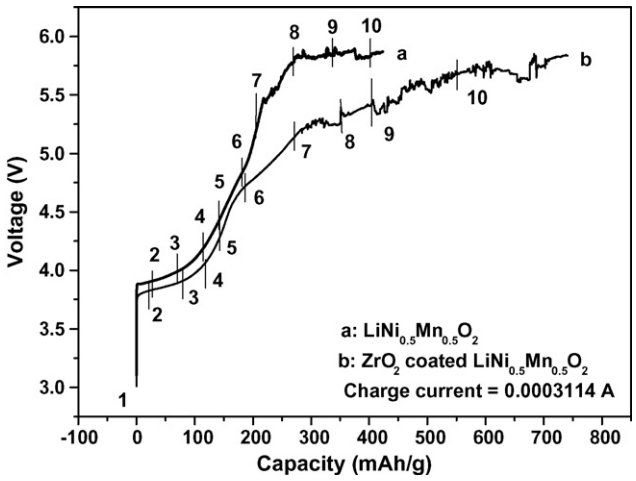


Fig. 1. The first charge curves of pristine and $ZrO_2$-coated $LiMn_{0.5}Ni_{0.5}O_2$ half cell from 2.5 to 5.7 V.

## 3. Results and discussion

The first charge curves of the pristine and the $ZrO_2$-coated $LiMn_{0.5}Ni_{0.5}O_2$ and the selected points for *in situ* XRD measurements are shown in Fig. 1. The cells were charged at a constant current of 0.3 mA in the potential range of 2.5–5.7 V. The charging potential for the $ZrO_2$-coated $LiMn_{0.5}Ni_{0.5}O_2$ compound is much slower than the pristine one, indicating that the polarization for the $ZrO_2$-coated $LiMn_{0.5}Ni_{0.5}O_2$ compound is much lower. Meanwhile, the potential fluctuation starts at the charge capacity of around 200 and 260 mAh $g^{-1}$ for the pristine and the $ZrO_2$-coated $LiMn_{0.5}Ni_{0.5}O_2$ compounds, respectively. It suggests that the $ZrO_2$ coating layer may impede the reaction between cathode material and electrolyte [11–13]. During the first charge, 10 XRD scans were continuously collected, as indicated as the selected points in Fig. 1.

The *in situ* XRD patterns of pristine $LiMn_{0.5}Ni_{0.5}O_2$ cathode materials are shown in Fig. 2 for the region with Bragg reflec-

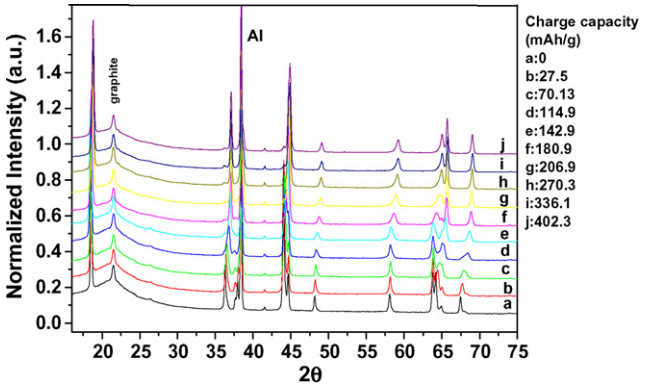


Fig. 2. *In situ* XRD patterns in the 16–75° 2$\theta$ range for pristine $LiMn_{0.5}Ni_{0.5}O_2$ cathode during the first charge with a 0.3 mA charging current.

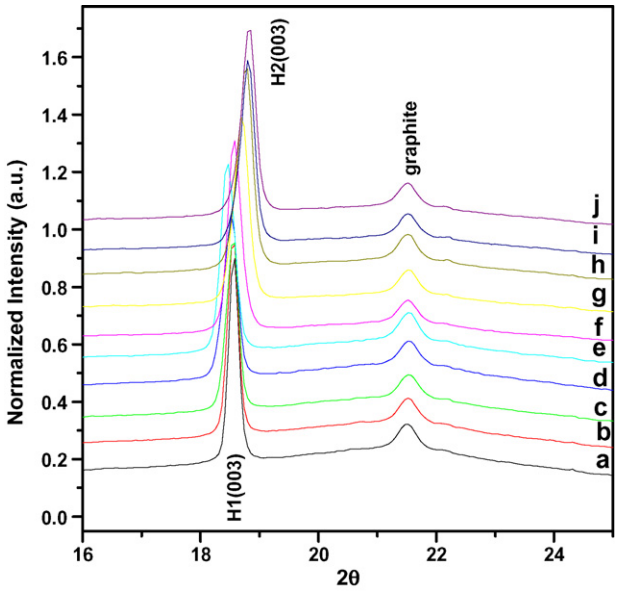


Fig. 3. *In situ* XRD patterns in the 16–25° 2$\theta$ range for pristine $LiMn_{0.5}Ni_{0.5}O_2$ cathode during the first charge with a 0.3 mA charging current. The 2$\theta$ angles have been converted to those corresponding to Cu Kα radiation (λ = 1.54 Å).

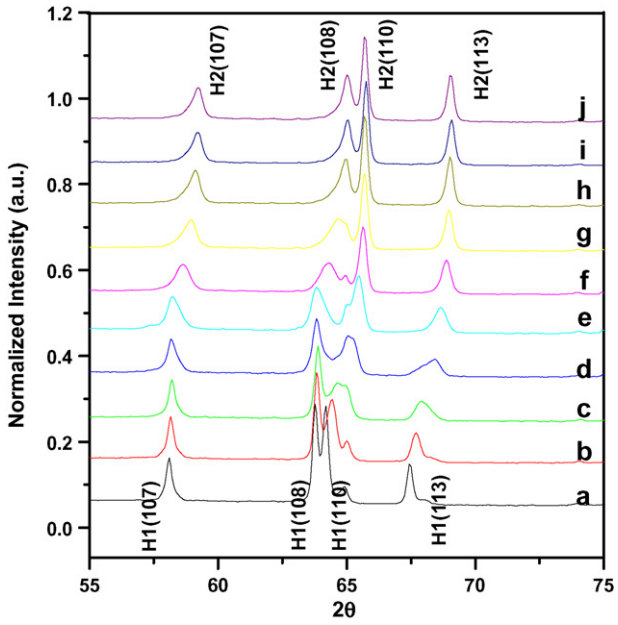


Fig. 5. *In situ* XRD patterns in the 55–75° 2$\theta$ range for pristine $LiMn_{0.5}Ni_{0.5}O_2$ cathode during the first charge with a 0.3 mA charging current.

tions. In order to check the phase transition, the *in situ* XRD patterns were divided into various 2$\theta$ regions such as 16–25°, 35–50° and 55–75° and were plotted in Figs. 3–5, respectively. For making comparison with XRD data collected using Cu $K_\alpha$ radiation, all XRD patterns are converted to those for a corresponding wavelength of λ = 1.54 Å in this study. Two hexagonal phases (H1, H2) can be identified and their corresponding Bragg peaks are indexed in these figures. An obvious phase transition in the pristine $LiMn_{0.5}Ni_{0.5}O_2$ can be found in Fig. 3, the phase converts from H1 to H2 at the charge capacity of about 142.9 mAh $g^{-1}$ (~4.4 V) and completely transfers to H2 phase at the charge capacity of about 206.9 mAh $g^{-1}$ (5.3 V). In this potential range H1 (1 0 1) and H1 (1 0 4) smoothly convert to H2 (1 0 1) and H2 (1 0 4), as shown in Fig. 4. By comparison these *in situ* XRD patterns, the structural change slowly at the beginning of the charge (a–d) and continuously convert to H2 phase as the charge capacity reaches 142.9 mAh $g^{-1}$ (e) and totally convert to H2 phase when the sample was charged to 206.9 mAh $g^{-1}$ (f, ~4.8 V).

For the purpose of investigation on the contribution of the $ZrO_2$ coating to its electrochemical performance, the $ZrO_2$-coated $LiMn_{0.5}Ni_{0.5}O_2$ cathode material was also examined by the *in situ* XRD to monitor its phase transition upon charge in the potential range of 2.5–5.7 V. The *in situ* XRD patterns of the $ZrO_2$-coated $LiMn_{0.5}Ni_{0.5}O_2$ cathode compounds were collected in Fig. 6 for the region with Bragg reflections. The structural change of the $ZrO_2$-coated $LiMn_{0.5}Ni_{0.5}O_2$ cathode material is more gentle than the pristine one. As shown in Fig. 7, the H1 (0 0 3) slowly (smoothly) coverts to H2 (0 0 3) upon charge. The (0 0 3) peak position slowly moves to low angle in the scans of a (OCP) to f (~4.6 V, 187.3 mAh $g^{-1}$) and then moves back to high angle again at the charge capacity of about 270.3 mAh $g^{-1}$ (~5.1 V). The phenomena can be seen in the other 2$\theta$ region; the (1 0 1), (1 0 4) and (1 0 5) phase continuously changes with an increase in the charging state as plotted

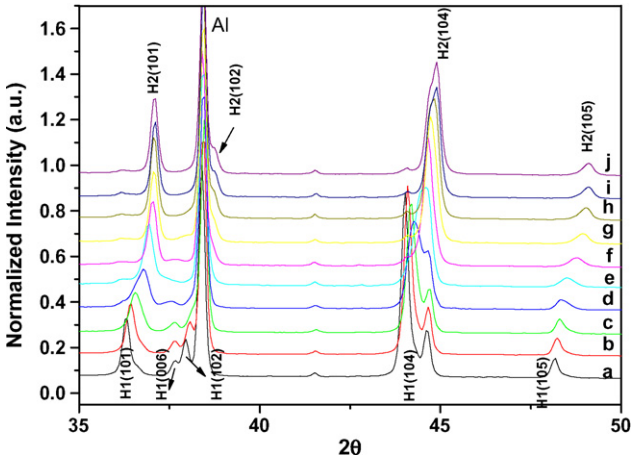


Fig. 4. *In situ* XRD patterns in the 35–50° 2$\theta$ range for pristine $LiMn_{0.5}Ni_{0.5}O_2$ cathode during the first charge with a 0.3 mA charging current.

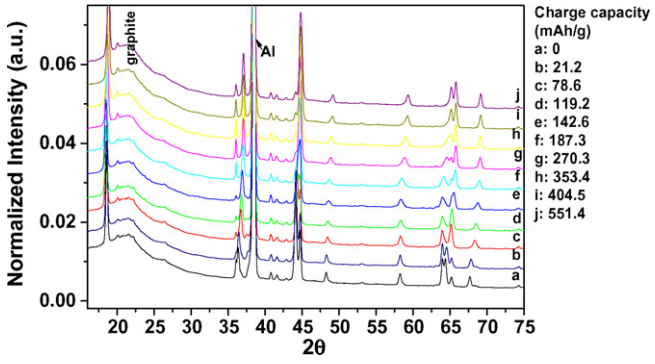


Fig. 6. *In situ* XRD patterns in the 16–75° 2$\theta$ range for $ZrO_2$-coated $LiMn_{0.5}Ni_{0.5}O_2$ cathode during the first charge with a 0.3 mA charging current.

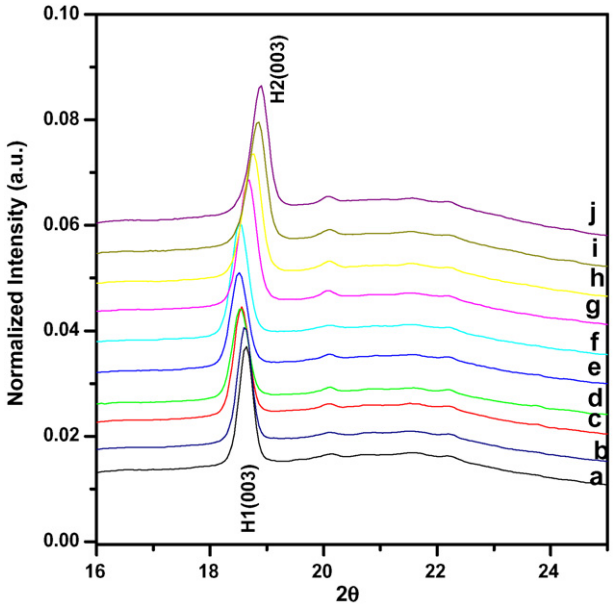


Fig. 7. *In situ* XRD patterns in the 16–25° 2$\theta$ range for $ZrO_2$-coated $LiMn_{0.5}Ni_{0.5}O_2$ cathode during the first charge with a 0.3 mA charging current.

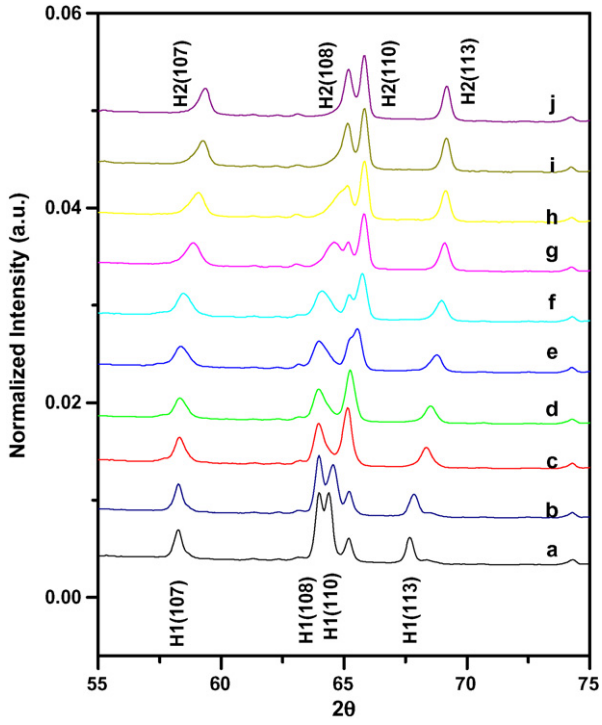


Fig. 9. *In situ* XRD patterns in the 55–75° 2$\theta$ range for $ZrO_2$-coated $LiMn_{0.5}Ni_{0.5}O_2$ cathode during the first charge with a 0.3 mA charging current.

in Fig. 8. In Fig. 9, the structural transformation process is also gentle. No drastic phase change can be found in the $ZrO_2$-coated $LiMn_{0.5}Ni_{0.5}O_2$ cathode material during charging process. The phase transition from H1 to H2 structure is complete when the $ZrO_2$-coated $LiMn_{0.5}Ni_{0.5}O_2$ cathode material was charged to 270 mAh $g^{-1}$ (g, ~5.3 V). No drastically phase transition can be discovered in the charging process even to 5.5 V.

To understand the volume change during the charging process of both samples, the lattice parameters were calculated from *in situ* XRD patterns and plotted in Fig. 10 (the corresponding charge capacity is described beside the figure. As seen in this figure, the *a*-axis length decreases as the charging capacity increases. The lattice parameter *a* for the pristine $LiMn_{0.5}Ni_{0.5}O_2$ cathode material decreases rapidly from 2.902 (±0.005) to 2.842 (±0.005) Å in the potential range of 2.93–5.11 V (187 mAh $g^{-1}$). Meanwhile, the parameter *a* for the $ZrO_2$-coated $LiMn_{0.5}Ni_{0.5}O_2$ cathode material decreases from 2.894 (±0.005) to 2.839 (±0.005) Å in the potential range of 2.93–4.3 V (180 mAh $g^{-1}$). When the lattice parameter *a* for the pristine and coated samples reaches 2.839 (±0.005) and 2.843 (±0.005) Å, the parameter *a* remains unchanged even the charging potential (charge capacity) increases further. In order to know the variation of parameter *c*, the lattice parameters *c* and *c*/*a* ratio are also calculated from the *in situ* XRD patterns. The lat-

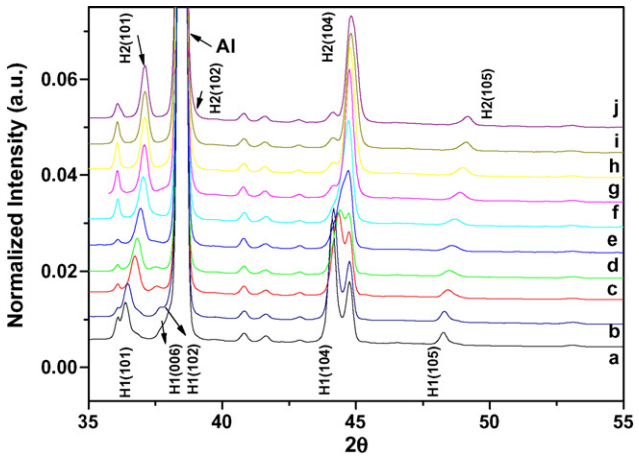


Fig. 8. *In situ* XRD patterns in the 35–55° 2$\theta$ range for $ZrO_2$-coated $LiMn_{0.5}Ni_{0.5}O_2$ cathode during the first charge with a 0.3 mA charging current.

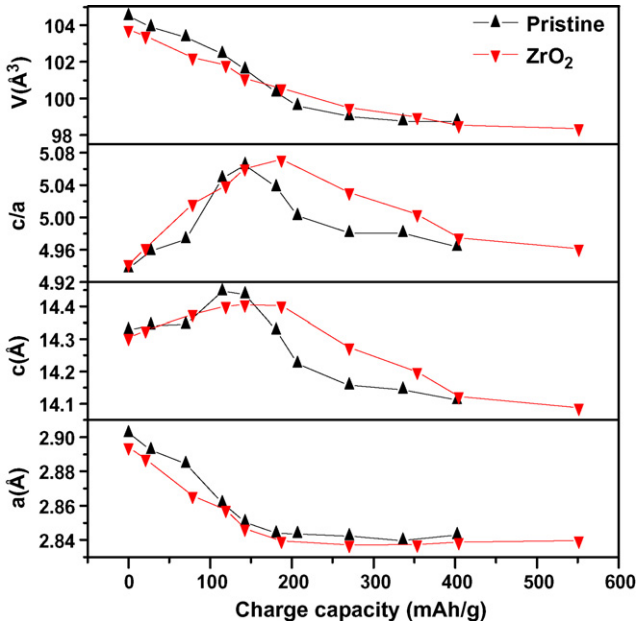


Fig. 10. The lattice parameters *a*, *c*, *c*/*a* and unit cell volume of the charged pristine and $ZrO_2$-coated $LiMn_{0.5}Ni_{0.5}O_2$ at various charged capacities.

tice parameters *c* and *c*/*a* ratio increase with an increase in the charging capacity. It reveals the *c*-axis expands when the layered cathode is charged at the beginning. During the $Li^+$ extraction process, the static force induces the increasing of *c*-axis expansion. However, the layered structure would collapse when the amount of the $Li^+$-extraction is too high. It results in the variation of *c*-axis during the charging process. It is interesting to compare the variations of the *c*-axis for the two cathode materials, the structure of the $ZrO_2$-coated $LiMn_{0.5}Ni_{0.5}O_2$ compound does not collapse until the charge capacity reach 180.9 mAh $g^{-1}$ but the *c*-axis of the pristine $LiMn_{0.5}Ni_{0.5}O_2$ compound begins to decrease at the charge capacity of about 142.9 mAh $g^{-1}$. It demonstrates that the $ZrO_2$ coating can stabilize the layered structure of the $LiMn_{0.5}Ni_{0.5}O_2$ compound. The similar phenomena can be also discovered in *c*/*a* ratio. The lattice parameter *a* decreases during the charging process and lattice parameter *c* also decreases when the charge potential is higher than 4.3 and 4.7 V for the pristine and $ZrO_2$-coated $LiMn_{0.5}Ni_{0.5}O_2$, respectively. Owing to the change of the lattice parameters, the volume of these samples decreases as the charge potential increases. The $ZrO_2$-coated $LiMn_{0.5}Ni_{0.5}O_2$ compound shows lower volume and lattice parameter change during the charging process. The $ZrO_2$ coating on the $LiMn_{0.5}Ni_{0.5}O_2$ compound not only impedes the decomposition reaction of electrolyte its surface but also restrains its structural change upon charge. It is believed that these two factors would mainly responsible for the improvement of its electrochemical performance.

## 4. Conclusion

The *in situ* XRD investigation was performed on the pristine and the $ZrO_2$-coated $LiMn_{0.5}Ni_{0.5}O_2$ cathode materials. From the observation of the start of potential fluctuation, it is believed that the $ZrO_2$-coating layer can impede the electrolyte decomposition on the surface of the cathode material. This coating layer on the $LiMn_{0.5}Ni_{0.5}O_2$ compound can extend its phase transition and prevent its structure from collapse at much higher charge capacity compared to the pristine one. *In situ* XRD study indicate the $ZrO_2$-coated $LiMn_{0.5}Ni_{0.5}O_2$ has higher structural stability than the pristine one. By comparison, the lattice parameter change of these cathode materials show the coating layer can reduce the lattice expansion during the charging process. It is believed that the inhibition of electrolyte decomposition on its surface and the stabilization of its layered structure are two major factors responsible for the improvement of its electrochemical performance for the coated-cathode material.

## Acknowledgements

The financial support from the Ministry of Education of Taiwan (EX-93-E-FA09-5-4), National Science Council of Taiwan (NSC-95-ET-7-011-002-ET), National Synchrotron Radiation Research Centre, and National Taiwan University of Science and Technology is acknowledged.

## References

[1] M.E. Spahr, P. Novak, O. Haas, R. Nesper, J. Power Sources 68 (1997) 629.
[2] Z. Lu, D.D. MacNeil, J.R. Dahn, Electrochem. Solid-State Lett. 4 (2001) A191.
[3] C.S. Johnson, S.D. Korte, J.T. Vaughey, M.M. Thackeray, T.E. Bofinger, Y. Shao-Horn, S.A. Hackney, J. Power Sources 81–82 (1999) 491.
[4] T. Ohzuku, Y. Makimura, Chem. Lett. (2001) 744.
[5] L. Zhang, H. Noguchi, M. Yoshio, J. Power Sources 110 (2002) 57.
[6] C.S. Johnson, J.S. Kim, A.J. Arthur, J. Kahaian, J.T. Vaughey, M.M. Thackeray, Electrochem. Commun. 4 (2002) 492.
[7] Z. Chen, J.R. Dahn, Electrochem. Solid-State Lett. 6 (2003) 221.
[8] X.Q. Yang, J. McBreen, W.S. Yoon, C.P. Grey, Electrochem. Commun. 4 (2003) 649.
[9] B.J. Hwang, R. Santhanam, D.G. Liu, J. Power Sources 97–98 (2001) 443.
[10] B.J. Hwang, R. Santhanam, D.G. Liu, J. Power Sources 101 (2001) 86.
[11] Z. Chen, J.R. Dahn, Electrochem. Solid-State Lett. 5 (2002) A213.
[12] J. Cho, Y.J. Kim, B. Park, J. Electrochem. Soc. 148 (2001) a1110.
[13] J. Cho, Y.J. Kim, B. Park, Chem. Mater. 12 (2000) 3788.